Synthesis, Characterization, and Tunable Optical Properties of Hollow Gold Nanospheres†

Adam M. Schwartzberg,‡,§ Tammy Y. Olson,‡,§ Chad E. Talley,§ and Jin Z. Zhang*,‡

Department of Chemistry and Biochemistry, University of California, Santa Cruz, California 95064, and Department of Chemistry and Materials Science, Lawrence Livermore National Laboratory, Livermore, California 94550

Received: April 5, 2006; In Final Form: May 5, 2006

Nearly monodisperse hollow gold nanospheres (HGNs) with tunable interior and exterior diameters have been synthesized by sacrificial galvanic replacement of cobalt nanoparticles. It is possible to tune the peak of the surface plasmon band absorption between 550 and 820 nm by carefully controlling particle size and wall thickness. Cobalt particle size is tunable by simultaneously changing the concentration of sodium borohydride and sodium citrate, the reducing and capping agent, respectively. The thickness of the gold shell can be varied by carefully controlling the addition of gold salt. With successful demonstration of ensemble as well as single HGN surface-enhanced Raman scattering, these HGNs have shown great potential for chemical and biological sensing applications, especially those requiring nanostructures with near-IR absorption.

Introduction

Nanostructured materials of coinage metals such as gold and silver have unique optical properties due to strong surface plasmon absorption in the visible region of light and provide excellent substrates for surface plasmon resonance (SPR) spectroscopy[1−9] and surface-enhanced Raman scattering (SERS).[10−19] The surface plasmon is a collective oscillation of conduction-band electrons within the nanoparticle induced by the oscillating dipole of a resonant wavelength of light.[20] The electron oscillation induces a surface electromagnetic (EM) field, which is largely responsible for the SERS effect.[21] The wavelength at which a given nanoparticle is resonant depends on the size, shape, chemical nature of the metal, and the embedding enviroment.[22−24]

In solid spherical particles, there is a single resonance at approximately 520 nm for gold and 400 nm for silver, varying slightly depending on size and embedding media. However, when one axis is extended, for example, a nanorod, the resonance will break into two absorption bands, one corresponding to the short axis, or transverse mode, and another to the long axis, or longitudinal mode.[25−28] The longitudinal mode has lower energy or redder absorption than the transverse mode. This is also true for aggregated systems in which there are multiple resonances within each given cluster of particles.[29−35] Therefore, controlling the size and shape of these metal nanostructures allows control of their optical properties that have potential applications in nanophotonics and sensing.

Control of the structure and thereby optical properties of gold and silver nanomaterials is especially important for SERS applications because the SERS enhancement factor depends on the optical absorption of the substrate.[11,36−38] Only nanostructures with absorption on-resonance with the incident light will contribute to the SERS signal, whereas those with absorption off-resonance with the incident light wavelength will contribute none or little to SERS.[39−42] In ensemble average experiments involving a large number of nanoparicles, optical and structural variations from particle to particle average out to yield consistent results from measurement to measurement. However, when examined at the single-nanoparticle or single-molecule level, the SERS spectrum and enhancement can vary significantly from one nanostructure to another because of their different structure and optical absorption. This is often complicated further by the necessity of aggregation of nanoparticles to achieve enhancements large enough for single-molecule observations.[39,40,42] Because aggregation is generally a random process, structural homogeneity is nearly impossible. It is essential to have high homogeneity or uniformity in the structure and optical absorption of the different nanostructures to achieve good consistency on a single nanostructure level. The solution to this is to design homogeneous SERS substrates that can provide significant single-particle enhancement without aggregation.

The first works to realize this goal were the so-called core/shell systems.[43,44] There are two major advantages of the core/shell system over standard solid gold or silver particles. First, because the synthesis of the core silica particle is well characterized, size tunable from 100 nm to more than a micrometer, and monodisperse, so is the resultant core/shell structure.[45] This leads to a nanostructure that is optically tunable from the visible to the IR and highly consistent on a particle-by-particle basis.[44] This is ideal for in situ biological studies because tissue has an absorption minimum in the IR. The second major advantage is their SERS response, even at the single-particle level.[46] Using a shell of gold or silver versus a solid particle allows the electromagnetic field to extend further from the surface, inducing greater enhancements than single, spherical particles.[43] There is also, most likely, some portion of the increased enhancement coming from surface roughness of the shells that is not present in the single particles. In these systems, the shell is most likely not single-crystalline and involves aggregates of nanoparticles.

† Part of the special issue "Charles B. Harris Festschrift".

* Corresponding author. E-mail: zhang@chemistry.ucsc.edu. Phone: (831) 459-3776. Fax: (831) 459-2935.

‡ University of California.

§ Lawrence Livermore National Laboratory.

10.1021/jp062136a CCC: $33.50
Published on Web 06/29/2006

As an effort to engineer so-called "hot spots" of large enhancement in single particles, Lee et al. produced nanocrescent structures by depositing silver over latex beads on a surface, then dissolving away the bead.[47] These hollow spheres are open-ended with a sharp edge, which greatly enhances the EM field. This engineered hot-spot approach yields improved SERS enhancements over core/shell systems and is of a similar homogeneity because of the highly consistent latex beads available. For applications requiring an extremely small probe size, however, both nanocrescents and core/shell systems are relatively large.

A system of particular interest where probe size is of utmost importance is intracellular studies.[48] It has been found that although particles larger than 100 nm can enter a cell they do not do so readily and may interrupt some cellular functions. Similarly, particles that are too small, less than 20 nm, will diffuse out of the cell, rendering them useless. The ideal is a structure that can be tuned in size between 20 and 100 nm depending on the application.

By utilizing sacrificial galvanic replacement of silver with gold, Xia et al. have produced nanostructures with tunable sizes and excellent optical properties.[49−52] This synthetic technique utilizes the redox potential between metallic silver and gold salt in solution. When the Au^{3+} ions come in contact with the silver atoms, there is an electroless plating that reduces the Au^{3+} ions to gold atoms and oxidizes the silver to Ag^{1+} ions. For every three silver atoms oxidized, a single gold atom is reduced, leading to structures with $^1/_3$ the metal, leaving a hollow core. Because the structure is no longer a solid sphere, the plasmon resonance is shifted from its normal position, similar to the core/shell systems. Recently, this work has been extended to hollow nanocubes, which have been shown to be SERS active, however, not at the single-particle level.[53]

We have shown that by using a similar technique developed by Liang et al.,[54] in which cobalt is used as the sacrificial template to create hollow gold nanospheres (HGNs), it is possible to observe SERS at the single-particle level with 30 nm HGNs.[55] Along with this single-particle sensitivity, we found significantly increased homogeneity over solid silver nanoparticle systems for the application of single-particle pH sensing using surface functionalization with a pH-sensitive probe molecule. However, only a single particle size with limited plasmon tunability was used in that study. The ideal substrate would be highly tunable in both size and resonance while maintaining homogeneity.

To achieve broad size tunability of this HGN system, size control of the cobalt sacrificial template is required. Although there have been significant advances in the production of small sized (∼5−10 nm) cobalt nanoparticles with incredible homogeneity,[56] there has been little work in the production of larger particles. The main instance of this work is by Kobayashi et al. who showed significant size control in the production of silica capped cobalt particles by varying the $CoCl_2$/citric acid ratio.[57] Citric acid is the capping agent that stabilizes the particles, and its concentration strongly affects the number of nucleation sites that initiate particle growth. The key to controlling particle size is in the concentration of nucleation sites. In general, at a given metal salt concentration, the more nuclei that are formed, the smaller the average particle size will be. This is a simple mass distribution argument; however, controlling the production of nuclei is not necessarily a simple matter.[58,59]

Since the early work by Turkevich et al. and later Frens et al.,[60,61] it has been understood that in a standard colloidal gold synthesis using the hot citrate reduction of chloroauric acid, the particle size may be controlled by the concentration of citrate. In general, citrate stabilizes the initially formed nuclei and the more citrate present the more nuclei will be stabilized. However, when trying to apply this logic to the aqueous synthesis of cobalt nanoparticles, it is a significantly more challenging task.

Because of the stability of the cobalt salt, the reduction cannot be done by citrate alone and a stronger reducing agent is required. In this case, sodium borohydride is used to reduce the salt and citrate is present only as a capping agent. In this work, we present the synthetic route necessary to control the particle size of the cobalt nanoparticles, which is reflected in the resultant HGN diameter. The inner diameter, or wall thickness, can be controlled by the amount of gold salt used, leading to complete control of the optical properties of particles ranging from 20 to 70 nm. This makes it possible to tune the peak of the surface plasmon band absorption between 550 and 820 nm. For a particular diameter and wall thickness, the absorption band is relatively narrow because of the near-monodisperse distribution, as determined by single-nanosphere scattering spectrum. These HGNs have been further demonstrated to be active SERS substrates with excellent consistency based on a single HGN SERS spectra.

Materials and Methods

Materials. Cobalt chloride hexahydrate (99.99%), chloroauric acid trihydrate (ACS reagent grade), trisodium citrate dihydrate (>99%), citric acid (99%), 4-mercaptobenzoic acid, and sodium borohydride (99%) were obtained from fisher scientific. All water used in the syntheses was 18 MΩ milli-Q filtered.

Cobalt Nanoparticle Synthesis. Cobalt nanoparticles were synthesized with the utmost attention paid to cleanliness and exclusion of air. All glassware was cleaned with alconox glassware detergent and then with aquaregia to ensure the removal of all adsorbates; it was then washed repeatedly with ultrapure water. To ensure completely air-free solutions, all solutions were vacuumed on a Schlenk line until gas evolution ceased and then bubbled with ultrapure argon for 10 minutes. This process was repeated twice to remove as much oxygen as possible from the reaction vessel.

Fast Addition of Cobalt Chloride. Water (100 mL*)* was placed into a three-neck flask with 100−800 μL of a 0.1 M solution of sodium citrate or citric acid and deoxygenated. To this, 100−800 μL of a fresly made 1 M sodium borohydride solution was added. With rapid magnetic stirring, 100 μL of a 0.4−0.6 M cobalt chloride solution was added. Hydrogen evolved immediately, and the solution changed from pale pink to brown/gray indicating the reduction of Co (II) into cobalt nanoparticles. This solution was allowed to react for between 15 and 60 min, (under constant argon flow) depending on sodium borohydride concentration, until hydrogen stopped evolving, indicating complete hydrolysis of the reductant. The addition of sodium borohydride and cobalt chloride was also performed in reverse order.

Slow Addition of Cobalt Chloride. Water (75 mL) was placed in a 500 mL three-neck flask with 400 μL of a 0.1 M solution of sodium citrate. Water (25 mL) with 100 μL of 0.4 M cobalt chloride was placed in a 250 mL three-neck flask. These two solutions were deoxygenated. To the 500 mL three-neck flask, 300−400 μL of a freshly prepared 1 M sodium borohydride solution was added. Using a cannula and argon gas to pressurize the 250 mL flask, the cobalt chloride solution was added dropwise at approximately 10 mL/min. During this addition, the solution slowly changed from colorless to brown/gray signifying cobalt particle formation. This solution was allowed to react for 25 min to completely hydrolyze the sodium borohydride.

Gold Shell Growth. Because of the ease with which sodium borohydride is able to reduce the gold salt, it is imperative that it be completely hydrolyzed before introducing gold. The presence of sodium borohydride is checked by halting stirring and inspecting the solution for bubbles, indicating the continuing hydrolysis of the reductant. It is only when bubbling has ceased completely that gold may be added.

High-Concentration Addition. Upon ensuring complete hydrolysis of the sodium borohydride, the flow of argon was increased and a 0.1 M solution of chloroauric acid was added at 50 μL/addition to a total volume between 150 and 450 μL. Between each addition, 30−60 s are allowed to pass to ensure complete mixing. Upon completion of gold addition, the argon flow was stopped and the vessel was opened to ambient conditions under rapid stirring to oxidize any remaining cobalt metal left in solution.

Low-Concentration Addition (Retaining Co at Core). Using a cannula, 30 mL of the sodium borohydride-free cobalt nanoparticle solution was transferred to an argon-purged graduated cylinder. This was then rapidly added to a vortexing 10 mL solution of chloroauric acid. The gold solution contained between 20 and 60 μL of cloroauric acid diluted to 10 mL. This solution may be kept under argon flow to retain the cobalt core; however, by exposing the solution to air the cobalt was completely oxidized, leaving only water and dissolved salts at the core of the HGN. Samples with remaining cobalt cores retain a brown color, whereas oxidized samples change to between purple- and green-colored depending on the amount of gold added and size of the particle.

Experimental Measurements. Low-resolution TEM measurements were performed on a JEOL model JEM-1200EX microscope, and high-resolution TEM was performed on a Philips CM300-FEG at the national center for electron microscopy at Lawrence Berkeley National Laboratory. Absorption measurements were taken on an HP 89532A spectrometer. All spectra were fit with Igor Pro 5.0 using a Lorentzian function with chi square values less than 0.1. Particles were sized with imageJ image processing software.[62]

SERS and Rayleigh scattering measurements were performed on a home-built confocal microscope system described previously[42] with the addition of transmitted light, dark field illuminator (NA 1−1.4). For SERS experiments, a Zeiss Apochromat 60 X, 1 NA air objective was used. Typically, the sample was integrated for 30 s with a total power of 100 μW from a helium−neon laser (632.8 nm, Melles Griot). Rayleigh scattering experiments were performed with a Zeiss Apochromat 100 X, 0.7 NA oil-emersion objective.

Samples for Rayleigh scattering were prepared by immobilizing the particles on glass coverslips with trimethoxy-[3-(methylamino)propyl]silane (APS) (Aldrich). Coverslips were cleaned prior to the silanization step by sonication in a 2% solution of Hellmanex, followed by 18 MΩ water. They were then submerged in a 5 mM aqueous solution of APS to deposit the tethering molecules. After 1−2 min, the coverslips were rinsed with water, dried under nitrogen, and 40 μL of the as-prepared particle solution was placed on one surface. After several seconds exposed to the solution, it was rinsed with water and then blown dry with nitrogen.

Results and Discussion

Effect of Cobalt Chloride, Sodium Borohydride, and Sodium Citrate Concentration on Particle Size. The goal of this study was to gain control of the cobalt particle size by aqueous solution chemical methods. Previous work on this system by Liang et al. focused more on the thickness of the shell to control its optical properties.[54] Although their work produced excellent results, further tunability is necessary to make the system as useful as possible. Initial attempts to reproduce the work of Liang did not yield satisfactory results. The particles obtained were inhomogeneous and significantly smaller than the 60 nm reported. In fact, using as close to the original synthesis as possible, ∼25 nm cobalt particles were obtained; however, with their method of gold addition only inhomogeneous, gray solutions were observed. Upon determining an improved method of gold addition, this yielded excellent results for single-particle SERS probes. However, there are many applications that may benefit from larger particle size and further red-shifted absorption, including SERS.

The other guiding hand in this work was provided by Kobayashi et al, who first reported this cobalt particle synthesis, but proceeded to cap the particles with silica shells to protect them from oxygen.[57] They found that as citrate concentration was reduced, particle size increased. This is consistent with colloidal gold and silver syntheses and is not an unreasonable claim. For this application, however, their trend did not hold true. A significant difference between this work and that of Kobayashi is the time at which the reaction could be halted. In their work, for large cobalt particles, they were forced to add the silica growth reagents almost immediately upon reduction of the cobalt salt. Any delay at low citrate concentration and the solutions would become unstable and flocculate. In this work, however, if the gold solution is added too quickly, it is immediately reduced by the remaining sodium borohydride instead of the cobalt particles. This leads to an unfortunate mess of nanoparticles. To achieve optimal particle growth, a significant amount of time must pass in order to allow the sodium borohydride to completely hydrolyze before the gold can be added.

This being said, it is also important to note that even at relatively high concentrations of citrate where the particles are still stable after some time there is little change in particle size by merely altering the citrate concentration. There may be a relatively simple explanation for this observation. Because the particle stability is directly related to the concentration of citrate, there may have been an aggregation affect responsible for the size increase observed previously. As citrate concentration is reduced, we have observed that the rate of aggregation increased. Therefore, when capping the particles immediately after reduction, they are likely halting the aggregation at different stages depending on citrate concentration. When concentration is low, a larger aggregate will be formed before the silica can stabilize it; at high concentration, a smaller aggregate will be present. This may be responsible for the lack of crystalline structure in the as-synthesized particles. By sintering them at high temperature, they are likely fused into one crystalline particle.

Why then, does citrate not affect particle size as strongly as previously thought? In the case of colloidal gold, the reduction is done by the relatively weak reductant, citrate. This reaction is slow, which allows for thermodynamic processes to control the formation of clusters. Only as many seed particles will be formed in the reaction as can be stabilized by the capping agent/reductant. This means that the capping agent concentration will have a strong effect on the number of seed particles and, hence, particle size. In the formation of cobalt particles, however, a much stronger reducing agent is required. Because sodium borohydride is a significantly stronger reductant than is technically required to reduce the cobalt salt to cobalt metal, the reduction is extremely fast, taking place in less than 1 min as

TABLE 1: Dependence of Particle Size on Sodium Borohydride Concentration[a]

volume 0.4 M $CoCl_2$ (μL)	volume 0.1 M citrate (μL)	volume 1 M $NaBH_4$ (μL)	particle size (nm)
100	400	400	31 ± 2
100	400	100	44 ± 5

[a] All reactions were performed in 100 mL of water. All particle sizes are determined by examining the resulting gold particles. Reported sizes are diameters.

opposed to 5−10 min for the reduction of gold salt by citrate. Because of this, kinetic processes dominate the formation of seed particles. The number of seeds, and therefore the size of the resulting particle, will be more dependent on the rate of the reduction.

The rate of reduction can be controlled in several ways. Temperature plays a strong role in the rate of reaction; however, little change in particle size was observed between particles synthesized at 0 °C and room temperature. A second way to alter rate is by changing the solution pH. The reductive potential of sodium borohydride is pH-dependent. It is important to note at this point that, contrary to previous reports of this synthesis, we use sodium citrate instead of citric acid. This is because the reaction was found to be slower at the higher pH, and particle homogeneity was superior in the neutral solution. Higher and lower pH was also attempted by adjusting with HCl and NaOH. These solutions, however, were unstable and immediately crashed out. This is most likely due to the presence of excess ions, especially Cl^-, which has a strong disrupting effect on aqueous colloidal capping. Finally, the concentration of reductant was used to change the reaction rate. This was found to be the best method of controlling particle size without drastically decreasing particle homogeneity.

By decreasing the amount of sodium borohydride present, the reaction time is increased substantially. This produces larger particles that remain stable in solution. Table 1 shows the result of varying sodium borohydride concentration by one-quarter. The particle size is increased by approximately 40%; however, this is the practical limit of size tunability by this method. Lower concentrations produce incredibly inhomogeneous results, which are often unstable. To form larger particles, we must also alter the sodium citrate concentration.

Although the sodium borohydride reduction of metal salts is largely kinetics-driven, there are still some thermodynamic-type processes controlling particle size. This is especially true as the concentration of reductant is decreased and the reaction is slowed. The reaction is now substantially more thermodynamically controlled, making the variation in capping-agent concentration more effective in controlling particle size. By decreasing both $NaBH_4$ and citrate concentration, we observed a drastic increase in particle size, this is shown in the 3D plot in Figure 1 and Table 2. The trend appears to be linear, at least within the concentrations shown here. At lower concentrations, the particle sizes could be substantially larger; however, because they crash out of solution almost immediately this is not something we could test. We present this as a general method of tuning the size of cobalt nanoparticles. Using this plot, it is possible to predict roughly what the final particle size will be at a given sodium borohydride and sodium citrate concentration.

Influence of the Rate of Addition and Concentration of $CoCl_2$ on Particle Homogeneity. Sample homogeneity is an important parameter to control, especially when focusing on optical properties. Inhomogeneous samples will have significantly broadened ensemble-averaged plasmon bands, making the sample less desirable for optical applications such as SERS. To increase particle homogeneity and size, a slow addition of low-concentration cobalt salt was attempted. It was thought that this would artificially slow the rate of reaction. This, however, was not the case, as is clear in Table 3. Although slightly larger particles were achieved, the coefficient of variation increases from 7% to 18%. This is clearly not an advantageous method of controlling particle size. The reason for this great increase

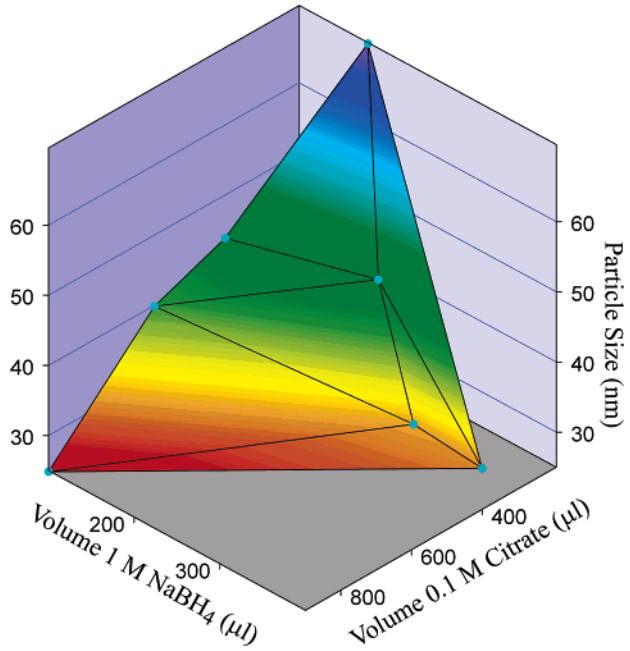

Figure 1. Particle size as a function of citrate and sodium borohydride concentration. All particle sizes are determined by examining TEM images of the resulting gold structures and represent the measurement of at least 200 particles. Reported sizes are diameters.

TABLE 2: Particle Size as a Function of Citrate and Sodium Borohydride Concentration Shown Illustratively in Figure 1[a]

particle diameter (nm)	volume 0.1 M citrate (μL)	volume 1 M $NaBH_4$ (μL)
71	190	180
46	330	250
44	400	100
36	600	100
31	400	400
28	400	320
25	900	100

[a] All reactions were performed in 100 mL of water. All particle sizes are determined by examining the resulting gold particles. Reported sizes are diameters.

TABLE 3: Influence of Rate of Addition and Concentration of Cobalt Salt on Particle Size[a]

rate of $CoCl_2$ addition	$CoCl_2$ concentration (M)	volume 0.1 M citrate (μL)	volume 1 M $NaBH_4$ (μL)	particle size (nm)
fast	0.4	400	400	28 ± 2
slow	0.4 (diluted)	400	400	31 ± 6
fast	0.5	400	400	50 ± 5

[a] All particle sizes are diameters. The cobalt chloride solution used for the slow addition is diluted to 25 mL with water.

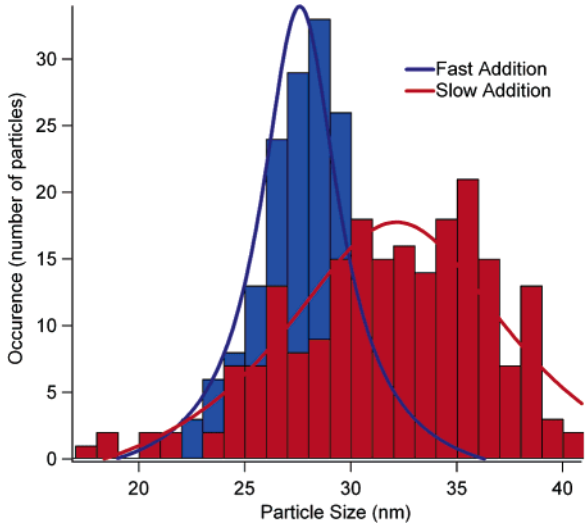

Figure 2. Histograms showing the size dispersion of cobalt nanoparticles produced by slow and fast addition of cobalt chloride. Solid lines are best fits demonstrating particle dispersion. Particles sizes are determined by measuring low-resolution TEM images.

in variation is due to the continual formation of seed particles as the cobalt is added. When examining the particles, it is obvious that some seeds are formed initially and result in very large particles, whereas others are formed throughout the addition and lead to small particles. This is clear in Figure 2, which shows histograms of particle size from slow and fast addition of cobalt. Not only does this exemplify the inhomogeneity of the slow addition sample but it also shows the asymmetric formation of particles. While the fast addition yields a nice, even sample, the slow addition yields a curve broadened and asymmetrically shifted by the presence of large particles formed early in the cobalt addition. This is clearly not the way to increase particle size. By increasing the concentration of cobalt while maintaining volume, however, we have found that particle size changes drastically without excessively broadening particle distribution; this is also clear in Table 3. Although higher concentrations of cobalt seem to induce flocculation, it may be possible to better control this with careful changes in citrate concentration.

Formation of Gold Shells. Along with the tunability of cobalt particle sizes, we have been able to produce a wide variety of sizes of the HGNs as shown in Figure 3. These are representative TEM images of the HGNs at different sizes. Figure 3A is a high-resolution TEM of a 30 nm particle; the lattice fringes of gold are clearly defined and show that these particles are polycrystalline with large single-crystalline areas. Figure 3B−F shows the tunability of the samples, from 70 to 28 nm. The largest particle sample in 3B clearly demonstrates the inhomogeneity that seems to be inherent at larger sizes. Also clear from these images, there is some very small (2−5 nm) gold particle formation in some samples. The origin of these particles is not entirely clear; however, they are more prevalent at high gold concentrations. They are likely a byproduct of the shell growth, small particles that do not grow into the shell, but break off early in the process.

Forming the gold shell seems to be an extremely simple matter at first glance; however, under closer inspection it becomes clear that there are many parameters that must be carefully controlled in order to form high-quality samples. As mentioned above, attempting to recreate the previous works did not result in good samples. Another method was needed to make

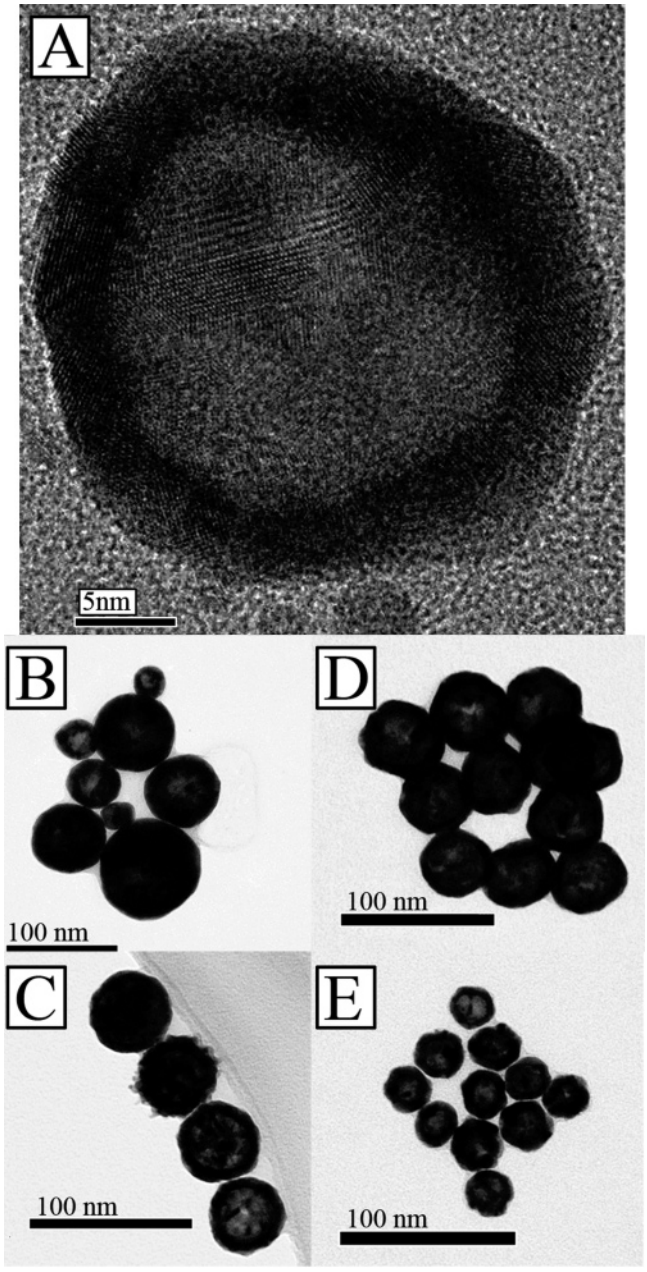

Figure 3. Transmission electron micrographs of the HGNs. (A) High-resolution TEM of a single 30 nm HGN. The wall thickness is approximately 4 nm and large areas of crystallinity are clearly visible. (B−E) Low-resolution TEM images of particles of 71 ± 17 nm (B), 50 ± 5 nm (C), 40 ± 3.5 nm (D), and 28 ± 2.3 nm.

homogeneous samples of high optical and structural quality like those shown in Figure 3.

High-Concentration Gold Addition. The general consensus on homogeneous nanoparicle formation is that a low concentration of reagents yields the best results. It is important to remember, however, that in the addition of gold here we are not forming a normal colloidal nanoparticle system. All that determines particle size and shape is the sacrificial template. For this reason, the high-concentration addition of gold should not necessarily produce poor results. After many failed attempts, it was found that by adding high-concentration (0.1 M) gold salt in small volumes yielded excellent results. Adding the gold all at once gave poor results, as did adding the solution dropwise. By using approximately 50 μL per addition over five to eight additions, spectrally narrow, optically dense samples were achieved.

The explanation for this is a fairly simple one; it is a matter of mixing. The reaction of gold salt with the cobalt particle is very fast, happening almost instantaneously upon the addition of the gold. There is also a secondary shell-mediated growth, which takes place on a slightly longer time scale, where free citrate in solution will reduce excess gold salt onto the formed shells. This can result in significantly thicker shells when too much gold is added. When a small amount of gold is introduced to the stirred solution, all particles at the site of the addition will immediately be oxidized completely in the presence of such a high-concentration gold. If there is excess gold at this site, then it will diffuse through the solution being reduced onto the cobalt particles until there is no more gold. If the volume of gold solution is too low, that is, dropwise, then the immediate impact will be relatively small, but due to the small size of the droplet it will dilute quickly. As the gold dilutes into the water, less and less will be reduced onto the cobalt, resulting in a gradient of shell thicknesses: thickest at the site of addition and thinner shells moving away from the concentration center. This leads to an incongruous sample in which some shells are badly underformed and some are overgrown by seed-mediated growth. An excellent example of this overgrowth is in Figure 3C. The second particle from the top has some slight overgrowth, which looks like small particle stuck to the surface. When the concentration is excessive, this becomes a much more pronounced feature of the particle.

At the other end of the addition rate scale is the all-at-once addition of the gold. This suffers similar problems to the dropwise addition; however, there is significantly more overgrowth, and less underformed particles. We were able to overcome this problem by using a middle of the road approach. By using 50 μL per addition, the resulting particles were uniform and we did not observe excessive overgrowth. The choice of this volume was not obvious and was discovered only by experimental trials. This method does, however, have one major flaw. Because such high concentrations are used, we were not able to readily control the shell thicknesses. In theory, if the gold is added correctly, the shell thickness should be a function of the amount of gold added. This was achieved by using relatively large volumes of low-concentration gold.

Low-Concentration Gold Addition. It was determined early on in this study that using low concentrations of gold would not produce satisfactory results; however, this assessment was not entirely correct. Several factors are required for the low-concentration addition of gold to work properly. The first is that the solution mix very well as quickly as possible. If the cobalt is added to the gold solution too slowly, then most of the gold will be utilized by a small number of particles, which will lead to poor sample homogeneity. Second, the volume of the gold salt to which the cobalt is added must be large enough that mixing can happen very quickly. With low volumes of gold at higher concentrations there is still a pronounced mixing problem, leading to poor samples. This is the problem we observed in reproducing the work of Liang et al. Although the larger volumes of gold produced reasonable results, using 5 or 8 mL of gold salt gave widely varying results and consistency was a major issue. Because mixing is the biggest issue in producing consistent results, it was hypothesized that by holding the volumes of gold and cobalt solutions constant, a more consistent result could be obtained.

By diluting varying volumes of gold salt to 10 mL with water and adding the cobalt as quickly as possible under rapid stirring we were able to produce homogeneous HGN with tunable wall thicknesses, similar to the work of Liang et al. Shell thickness varies linearly with gold concentration, indicating that homogeneous mixing is taking place, as shown in Table 4. These are representative values from a single sample and are consistent with all other data.

TABLE 4: Wall Thickness as a Function of the Volume of Gold Salt Added

volume of 0.1 M $HAuCl_4$ diluted to 10 mL (μL)	volume 0.1 M $CoCl_2$ (μL)	volume 0.1 M citrate (μL)	volume 1 M $NaBH_4$ (μL)	particle size (nm)	wall thickness
25	100	600	100	40 ± 6	6.2 ± 0.6
35	100	600	100	40 ± 6	6.9 ± 0.8
60	100	600	100	40 ± 6	8 ± 0.7

Effect of Particle Size and Wall Thickness on Optical Properties. One of the major intents of all this size tuning is the control of the optical properties of the HGN. We have found that by varying wall thickness and particle size it is possible to tune the plasmon absorption across much of the visible spectrum as in Figure 4a, UV−vis data, and 4b, an image of HGN solutions to illustrate the possible color range. These spectra are representative of many experiments and show the full range of tunability of this system. Although the full width at half-maximum (FWHM) of the spectra remains relatively unchanged from 500 to 750 nm and between 50 and 100 nm, the last two spectra are fairly broadened to over 200 nm. This is likely due to the formation of gold shells and their aggregates. At large particle size, there is less capping agent to stabilize the colloids. This likely brings about aggregation, which will significantly shift the absorption of the shells. The weak shoulder at 700 nm may be due to the presence of single shells, whereas the peak is due to the aggregates. At this time, however, it is not possible to determine the exact effect of the presence of the aggregates.

By increasing particle size at a constant wall thickness, the absorption band will red-shift as the plasmon oscillation decreases in energy. However, increasing wall thickness at constant particle size will blue-shift the absorption band. The band shifts to higher energy because as the inner diameter of the HGN decreases it takes on more solid-particle-like properties. Because solid gold particles at these sizes have plasmon bands at approximately 520 nm, the absorption will always shift in this direction as wall thickness increases. This is predicted in the work of Schatz et al. is shown experimentally here in Figure 5a and b.[23] These plots show the affect of the aspect ratio of particle size and wall thickness on plasmon absorption (a) as well as the affect of particle size and wall thickness on plasmon absorption. Representing 13 independent experiments, the trend is clearly shown here. Because the work of Schatz et al. is for particles of different sizes than those made here, we are not able to directly correlate their results to our data. However, we are currently working on similar calculations that should determine if these results match well to the theory.

Because wall thickness plays such an important role in the position of the plasmon absorption, it is important to understand how this corresponds to the amount of gold added to the solution. Figure 6 shows the nonnormalized absorption spectra of three samples made from a single batch of 35 nm cobalt nanoparticles. The highest concentration sample, at 60 μL of 0.1 M gold salt added absorbs most strongly at 638 nm, is the most blue-shifted of the three as would be expected and has a wall thickness of 7 ± 0.8 nm. The lower concentration samples at 35 and 25 μL are red shifted to 685 nm (wall thickness 5.6 $\pm$ 0.6 nm) and 702 nm (wall thickness 3.7 $\pm$ 0.6 nm), respectively. Interestingly, as the band shifts the fwhm changes only slightly from 80 nm for the 60 μL sample, to 91 nm for

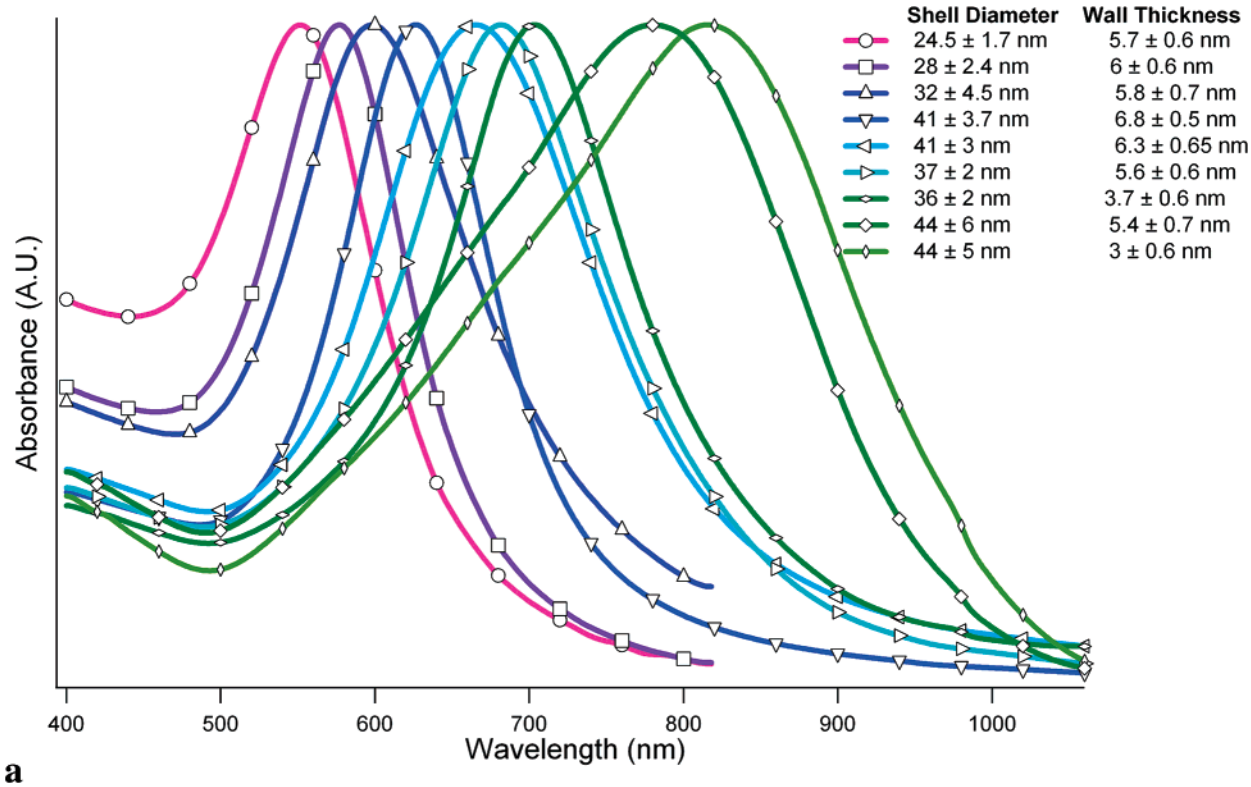

Figure 4. (a) UV−visible absorption spectra of nine HGN samples with varying diameters and wall thicknesses. (b) Image showing the color range of HGN solutions. The vial on the far left contains solid gold nanoparticles, the rest are HNGs with varying diameters and wall thicknesses.

the 35 μL sample, and to 82 nm for the 25 μL sample. This is not the trend one might expect given the propensity of solid gold nanoparticles to broaden significantly in spectrum with increasing size. This broadening is due to the introduction of new multipole modes, which are nonradiative and broader in energy than the normal dipole plasmon mode.[63,64] In fact, upon close examination of Figure 4a, it is clear that with the exception of the last two spectra, the FWHM changes little regardless of particle size or shell thickness. The explanation for this is tied to the electron mean free path in gold. Because the wall thickness is much less than this length (~50 nm), longer axes will dominate the plasmon oscillations and the multipole modes that appear in large particles will be minimized. Interestingly, this also explains why only one absorption band is observed for this system, whereas nanorods, which also have multiple axes of oscillation, will show two.

It may be noted that as the concentration of gold added decreases there is a decrease in optical density as well. This is not a matter of particle concentration, because 10 mL of gold is added to each sample, and the total number of HGNs is fixed to the number of cobalt particles present in the original solution. This is a function of absorption cross section of the HGNs due

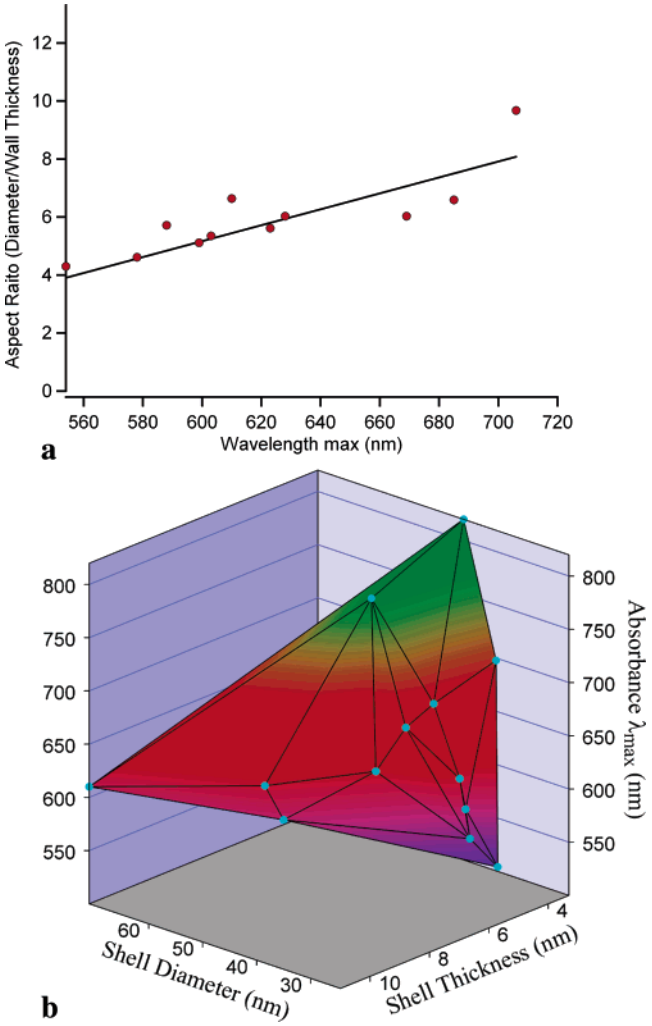

Figure 5. (a) Plasmon absorbance maximum wavelength (λ_{max}) as a function of the aspect ratio of shell thickness and shell diameter. The line is a best-fit approximation to guide the eye. (b) 3D plot of plasmon absorbance maximum wavelength (λ_{max}) as a function of the shell thickness and shell diameter. Each point on both plots represents an individual set of experiments and the average measured lengths.

to the different thicknesses of gold. As the wall grows thicker, it will have a larger absorption cross section.

Homogeneous Line Width and Inhomogeneous Broadening. To determine if, and to what extent, the absorption spectrum is broadened by inhomogeniety in the sample, we examined the Rayleigh scattering spectra of the HGNs. Although the FWHM of the ensemble-averaged solution of 30 ± 2.6 nm particles is 75 nm, the single-particle FWHM is 47 nm as shown in Figure 7. This is a broadening of 27 nm, which shows that the samples are slightly inhomogeneously broadened. This is to be expected to some point but is impressively small considering how sensitive these structures are to variance in wall thickness and local environment.[65,66] The sensitivity to local environment is clear upon examination of the spectral shift between the ensemble-averaged and scattering spectra. This is a shift of 14 nm and is consistent with all particles examined. The scattering spectra were taken from particles immobilized on glass substrates in air while the ensemble-averaged spectra were taken in aqueous solution. The refractive index of the imbedding medium decreases from 1.33 to 1 in going from water to air in these two scenarios. This substantially changes the optical properties of the HGNs. However, a decrease in refractive index has been shown to correspond to a blue shift.

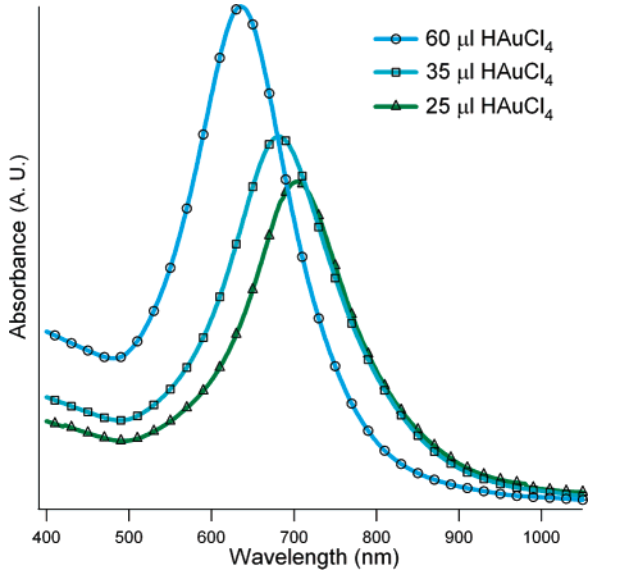

Figure 6. Spectral dependence on volume of added gold salt. Gold solutions were diluted to 10 mL with water before 30 mL of a cobalt solution made by the fast cobalt addition method with 100 μL sodium borohydride and 600 μL of citric acid. Average particle size is 35 ± 2 nm.

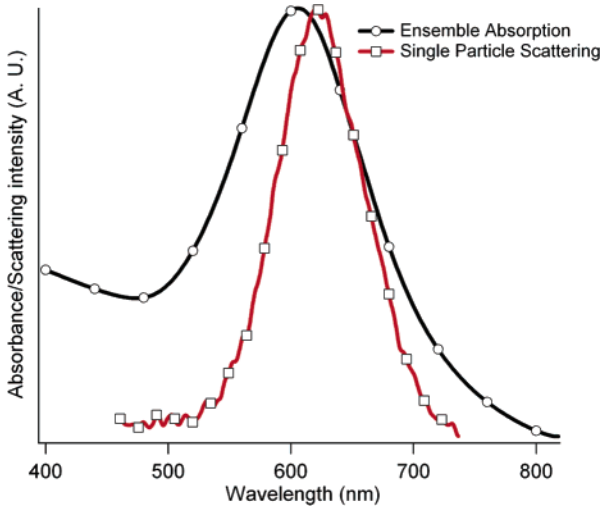

Figure 7. Comparison of ensemble-averaged absorption and single-particle Rayleigh scattering of 30 ± 2.6 nm HGNs.

It is not entirely clear why we observe a red shift from the ensemble-averaged sample; however, one possibility is the effect of particle immobilization to the glass slide. Although the ensemble-averaged solution particles are completely surrounded by water, the single particles were on a glass slide, partially surrounded by air, residual water, and glass. The cumulative effect of this compound refractive index may be enough to explain this anomalous red shift in the spectrum. Further studies are currently underway to better understand this effect.

Surface-Enhanced Raman Scattering. SERS experiments were performed on solutions of as-prepared HGNs with mercaptobenzoic acid (MBA) added to a final concentration of 1 mM. Although MBA tends to oxidize to form disulfides in aqueous solution, only fresh solutions were used to perform these studies. This should leave the thiol group free for binding to the gold surface or possibly cobalt. Solutions are normally washed to remove excess Co^{2+}; however, some may remain. This may cause sensitivity problems and is currently under investigation.

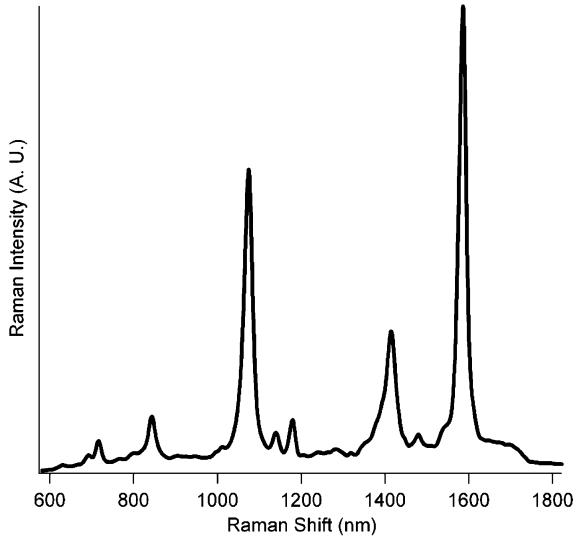

Figure 8. Ensemble-averaged surface-enhanced Raman scattering spectrum of mercaptobenzoic acid on the HGNs.

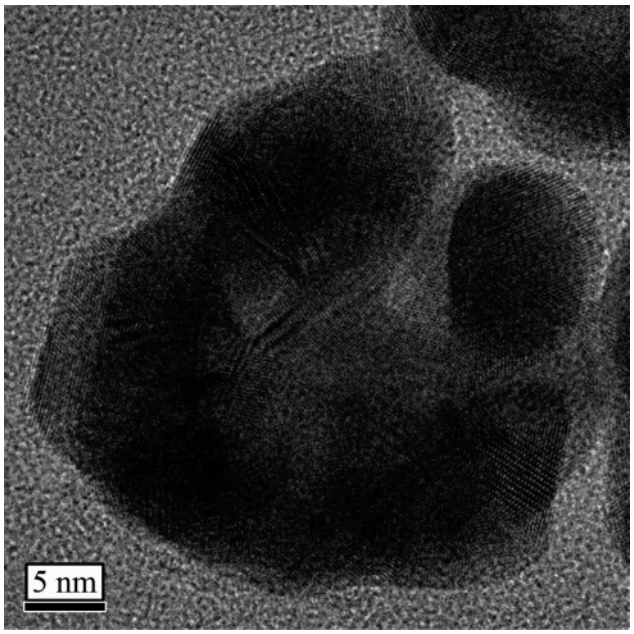

Figure 9. High-resolution TEM of an HGN formed from a slightly oxidized cobalt particle.

At this concentration of MBA, there was no spectral shift observed, which would indicate aggregation; therefore, we can nominally say that the resulting spectra are from nonaggregated or at least minimally aggregated HGNs. This was confirmed in our previous work on SERS of single HGNs, which showed that enhancement is observable from nonaggregated HGNs.[55] Here we show the ensemble-averaged SERS spectrum of MBA in Figure 8. In terms of enhancement, when compared in SERS intensity to aggregated Lee and Meisel silver particles, the standard high-enhancement SERS substrate, we achieve about 10% of the signal. This is an excellent result for nominally nonaggregated particles and significantly better than many current single-particle systems.

Avoiding Oxygen at All Costs. Finally, a few words about the effects of oxygen on HGN formation. Cobalt is extremely sensitive to oxygen, especially in aqueous solution. If the solution is not properly deoxygenated, or if air is allowed to enter the reaction vessel, then the results can be disastrous. Although it is still possible to perform the reduction of gold salt on partially oxidized cobalt particles, it produces very poor results. The physical result of this is shown in Figure 9. Although the oxidized cobalt will dissolve in the solution, it does not oxidize homogeneously, which results in malformed HGNs. Optically, this has extremely deleterious results greatly broadening the absorption band due to the random nature of the oxidation. When solutions are badly oxidized, the percentage of these types of particles tends to increase.

Conclusions

Nearly monodisperse HGNs of tunable interior and exterior diameter have been synthesized by sacrificial galvanic replacement of cobalt nanoparticles. We have been able to control the position of the surface plasmon band between 550 and 820 nm by carefully controlling particle size and wall thickness. Cobalt particle size, the sacrificial template that controls the resulting HGN size, is tunable by simultaneously changing the concentration of sodium borohydride and sodium citrate, the reductant and capping agent, respectively. This varies from all previously reported aqueous syntheses of cobalt particles. We also show that by controlling the addition of gold carefully the thickness of the gold shell can be varied. These HGNs have been further demonstrated to be excellent SERS substrates in terms of spectral consistency. They are promising for chemical and biological sensing applications, particularly those requiring near-IR absorption.

Acknowledgment. We thank Luis Liz-Marzán for useful discussions, and we appreciate financial support from the National Science Foundation, the Petroleum Research Fund/American Chemical Society, the University of California at Santa Cruz, the student employee graduate research fellowship at Lawrence Livermore National Laboratory, the Center for Biophotonics Science and Technology at the University of California at Davis, and the Genomics:GtL program of the Office of Science of the U.S. Department of Energy. The Center for Biophotonics, an NSF Science and Technology Center, is managed by the University of California, Davis, under Cooperative Agreement No. PHY 0120999. This work was performed under the auspices of the U.S. Department of Energy by University of California Lawrence Livermore National Laboratory under contract No. W-7405-Eng-48.

Note Added after ASAP Publication. This article was released ASAP on June 29, 2006. Figure 6 and references 34 and 55 have been revised. The correct version was posted on August 9, 2006.

References and Notes

(1) Sherry, L. J.; Chang, S. H.; Schatz, G. C.; Van Duyne, R. P.; Wiley, B. J.; Xia, Y. N. *Nano Lett.* **2005**, *5*, 2034.

(2) Hicks, E. M.; Zhang, X. Y.; Zou, S. L.; Lyandres, O.; Spears, K. G.; Schatz, G. C.; Van Duyne, R. P. *J. Phys. Chem. B* **2005**, *109*, 22351.

(3) Whitney, A. V.; Elam, J. W.; Zou, S. L.; Zinovev, A. V.; Stair, P. C.; Schatz, G. C.; Van Duyne, R. P. *J. Phys. Chem. B* **2005**, *109*, 20522.

(4) Haes, A. J.; Hall, W. P.; Van Duyne, R. P. *Laser Focus World* **2005**, *41*, 105.

(5) Lahav, M.; Vaskevich, A.; Rubinstein, I. *Langmuir* **2004**, *20*, 7365.

(6) He, L.; Smith, E. A.; Natan, M. J.; Keating, C. D. *J. Phys. Chem. B* **2004**, *108*, 10973.

(7) Penn, S. G.; He, L.; Natan, M. J. *Curr. Opin. Chem. Biol.* **2003**, *7*, 609.

(8) Nenninger, G. G.; Tobiska, P.; Homola, J.; Yee, S. S. *Sens. Actuators, B* **2001**, *74*, 145.

(9) Yee, S. S.; Homola, J.; Gauglitz, G. *Sens. Actuators, B* **1999**, *54*, 1.

(10) Creighton, J. A. Metal Colloids. In *Surface Enhanced Raman Scattering*; Chang, R. K., Furtak, T. E., Eds.; Plenum Press: New York, 1982; p 315.

(11) Moskovits, M. *Rev. Mod. Phys.* **1985**, *57*, 783.
(12) Yonzon, C. R.; Stuart, D. A.; Zhang, X. Y.; McFarland, A. D.; Haynes, C. L.; Van Duyne, R. P. *Talanta* **2005**, *67*, 438.
(13) Tian, Z. Q. *J. Raman Spectrosc.* **2005**, *36*, 466.
(14) Haynes, C. L.; Yonzon, C. R.; Zhang, X. Y.; Van Duyne, R. P. *J. Raman Spectrosc.* **2005**, *36*, 471.
(15) Kneipp, K.; Kneipp, H.; Itzkan, I.; Dasari, R. R.; Feld, M. S. *Chem. Rev.* **1999**, *99*, 2957.
(16) Nie, S. M.; Emery, S. R. *Science* **1997**, *275*, 1102.
(17) Otto, A. *J. Raman Spectrosc.* **2005**, *36*, 497.
(18) Otto, A.; Mrozek, I.; Grabhorn, H.; Akemann, W. *J. Phys.: Condens. Matter* **1992**, *4*, 1143.
(19) Campion, A.; Kambhampati, P. *Chem. Soc. Rev.* **1998**, *27*, 241.
(20) Quinten, M. *Appl. Phys. B* **2001**, *73*, 317.
(21) Moskovits, M. *J. Raman Spectrosc.* **2005**, *36*, 485.
(22) Creighton, J. A.; Eadon, D. G. *J. Chem. Soc., Faraday Trans.* **1991**, *87*, 3881.
(23) Hao, E.; Li, S. Y.; Bailey, R. C.; Zou, S. L.; Schatz, G. C.; Hupp, J. T. *J. Phys. Chem. B* **2004**, *108*, 1224.
(24) Link, S.; El-Sayed, M. A. *Annu. Rev. Phys. Chem.* **2003**, *54*, 331.
(25) Nikoobakht, B.; El-Sayed, M. A. *Chem. Mater.* **2003**, *15*, 1957.
(26) Chang, S. S.; Shih, C. W.; Chen, C. D.; Lai, W. C.; Wang, C. R. C. *Langmuir* **1999**, *15*, 701.
(27) Brioude, A.; Jiang, X. C.; Pileni, M. P. *J. Phys. Chem. B* **2005**, *109*, 13138.
(28) Yu, Y. Y.; Chang, S. S.; Lee, C. L.; Wang, C. R. C. *J. Phys. Chem. B* **1997**, *101*, 6661.
(29) Grant, C. D.; Schwartzberg, A. M.; Norman, T. J.; Zhang, J. Z. *J. Am. Chem. Soc.* **2003**, *125*, 549.
(30) Quinten, M. *J. Cluster Sci.* **1999**, *10*, 319.
(31) Quinten, M. *Appl. Phys. B.* **2000**, *70*, 579.
(32) Quinten, M.; Kreibig, U. *Appl. Opt.* **1993**, *32*, 6173.
(33) Schwartzberg, A. M.; Grant, C.; Wolcott, A.; Bogomolni, R.; Zhang, J. Z. *SPIE Proc.* **2003**, *5221*−*21*, 100.
(34) Norman, T. J.; Grant, C. D.; Schwartzberg, A. M.; Zhang, J. Z. *Opt. Mat.* **2005**, *27*, 1197.
(35) Kreibig, U. *Optical Properties of Metal Clusters*; Springer: Berlin; New York, 1995; Vol. 25.
(36) Kneipp, K.; Kneipp, H.; Itzkan, I.; Dasari, R. R.; Feld, M. S. *J. Phys.: Condens. Matter* **2002**, *14*, R597.
(37) McFarland, A. D.; Young, M. A.; Dieringer, J. A.; Van Duyne, R. P. *J. Phys. Chem. B* **2005**, *109*, 11279.
(38) Schatz, G. C.; Van Duyne, R. P. *Electromagnetic Mechanism of Surface-Enhanced Spectroscopy*; John Wiley and Sons Ltd.: Chichester, U.K., 2002.
(39) Brus, L. *Abstr. Papers Am. Chem. Soc.* **2001**, *221*, 112.
(40) Michaels, A. M.; Jiang, J.; Brus, L. *J. Phys. Chem. B* **2000**, *104*, 11965.
(41) Jiang, J.; Bosnick, K.; Maillard, M.; Brus, L. *J. Phys. Chem. B* **2003**, *107*, 9964.
(42) Schwartzberg, A. M.; Grant, C. D.; Wolcott, A.; Talley, C. E.; Huser, T. R.; Bogomolni, R.; Zhang, J. Z. *J. Phys. Chem. B* **2004**, *108*, 19191.
(43) Jackson, J. B.; Westcott, S. L.; Hirsch, L. R.; West, J. L.; Halas, N. J. *Appl. Phys. Lett.* **2003**, *82*, 257.
(44) Oldenburg, S. J.; Westcott, S. L.; Averitt, R. D.; Halas, N. J. *J. Chem. Phys.* **1999**, *111*, 4729.
(45) Halas, N. *Gold Bull.* **2004**, *37*, 137.
(46) Talley, C. E.; Jackson, J. B.; Oubre, C.; Grady, N. K.; Hollars, C. W.; Lane, S. M.; Huser, T. R.; Nordlander, P.; Halas, N. J. *Nano Lett.* **2005**, *5*, 1569.
(47) Lu, Y.; Liu, G. L.; Kim, J.; Mejia, Y. X.; Lee, L. P. *Nano Lett.* **2005**, *5*, 119.
(48) Chithrani, B. D.; Ghazani, A. A.; Chan, W. C. W. *Nano Lett.* **2006**, *6*, 662.
(49) Chen, J. Y.; Wiley, B.; McLellan, J.; Xiong, Y. J.; Li, Z. Y.; Xia, Y. N. *Nano Lett.* **2005**, *5*, 2058.
(50) Wiley, B.; Sun, Y. G.; Chen, J. Y.; Cang, H.; Li, Z. Y.; Li, X. D.; Xia, Y. N. *MRS Bull.* **2005**, *30*, 356.
(51) Wiley, B.; Sun, Y. G.; Mayers, B.; Xia, Y. N. *Chem.*—*Eur. J.* **2005**, *11*, 454.
(52) Sun, Y. G.; Mayers, B.; Xia, Y. N. *Adv. Mater.* **2003**, *15*, 641.
(53) McLellan, J. M.; Xiong, Y. J.; Hu, M.; Xia, Y. N. *Chem. Phys. Lett.* **2006**, *417*, 230.
(54) Liang, H. P.; Wan, L. J.; Bai, C. L.; Jiang, L. *J. Phys. Chem. B* **2005**, *109*, 7795.
(55) Schwartzberg, A. M.; Oshiro, T. Y.; Huser, T. R.; Zhang, J. Z.; Talley, C. E. *Anal. Chem.* **2006**, *78*, 4732.
(56) Lisiecki, I.; Pileni, M. P. *Langmuir* **2003**, *19*, 9486.
(57) Kobayashi, Y.; Horie, M.; Konno, M.; Rodriguez-Gonzalez, B.; Liz-Marzan, L. M. *J. Phys. Chem. B* **2003**, *107*, 7420.
(58) Chow, M. K.; Zukoski, C. F. *J. Colloid Interface Sci.* **1994**, *165*, 97.
(59) Biggs, S.; Chow, M. K.; Zukoski, C. F.; Grieser, F. *J. Colloid Interface Sci.* **1993**, *160*, 511.
(60) Turkevich, J.; Stevenson, P. C.; Hiller, J. *Discuss. Faraday Soc.* **1951**, *11*, 55.
(61) Frens, G. *Nat. Phys. Sci.* **1973**, *241*, 20.
(62) Abramoff, M. D.; Magelhaes, P. J.; Ram, S. J. *Biophotonics Int.* **2004**, *11*, 36.
(63) Payne, E. K.; Shuford, K. L.; Park, S.; Schatz, G. C.; Mirkin, C. A. *J. Phys. Chem. B* **2006**, *110*, 2150.
(64) Millstone, J. E.; Park, S.; Shuford, K. L.; Qin, L. D.; Schatz, G. C.; Mirkin, C. A. *J. Am. Chem. Soc.* **2005**, *127*, 5312.
(65) Nehl, C. L.; Grady, N. K.; Goodrich, G. P.; Tam, F.; Halas, N. J.; Hafner, J. H. *Nano Lett.* **2004**, *4*, 2355.
(66) Sun, Y. G.; Xia, Y. N. *Anal. Chem.* **2002**, *74*, 5297.